

WELL-CONTROLLABLE TURBULENCE GENERATOR USING A BIAXIALLY ROTATING SPHERE

Susumu Goto, Shigeo Kida, Michio Nishioka, Nobukazu Ishii, and Kentaro Nakayama
 Department of Mechanical Engineering and Science, Kyoto University
 Yoshida-Honmachi, Sakyo, Kyoto, 606-8501, Japan
 goto@mech.kyoto-u.ac.jp

ABSTRACT

We propose a tabletop turbulence generator using a biaxially rotating (i.e. precessing) sphere. The flow inside the sphere is governed by two well-controllable parameters related with the spin and the precession angular velocities. The time-series analysis of PIV data for the velocity field reveals that turbulence is sustained even with a weak precession as far as the spin is sufficiently fast. We show the three-dimensional spatial flow structures obtained by the direct numerical simulations at the precisely same conditions as laboratory experiments.

INTRODUCTION

One of our dreams in the turbulence research is to control turbulence (so as to enhance mixing or suppress drag, for instance) by a simple means such as tuning external flow conditions. As a fundamental step towards this dream, we here propose a compact turbulence generator in which the external conditions are precisely controlled so that high flow reproducibility can be ensured. What we have used for this purpose is a biaxially rotating sphere (Fig. 1). We rotate a sphere filled with a fluid at a constant angular velocity Ω_s around a horizontal axis (the spin axis) on a turntable which rotates at a constant angular velocity Ω_p around a vertical axis (the precession axis). Note that the spin axis rotates around the precession axis in the laboratory frame. One of the most important characteristics of this flow system is that no uncertainty in external conditions comes in if and only if these two angular velocities are precisely controlled.

By the way, it must be emphasised that flows inside a precessing cavity such as sphere, spherical shell, spheroid, spheroidal shell, and cylinder have been extensively investigated by many authors (Busse 1968, Hollerbach and Kerswell 1995, Kerswell 1995, Koblentz 1995, 1996, Lorenzani and Tilgner 2001, Manasseh 1992, Noir *et al.* 2001, 2003, Tilgner and Busse 2001, Vanyo *et al.* 1995, 2000) mainly from the geophysical viewpoint since the seminal work by Malkus (1968). Malkus, actually, carried out a similar laboratory experiment to ours in order to show the possibility of the dynamo action due to the turbulent flow of the Earth's outer core (melted iron) which is confined in the spheroidal mantle. Recall that the earth is precessing with the period of about 26000 years. He demonstrated that turbulence can be sustained even with a weak precession. This claim that turbulence is easily sustained by such a weak action is not only interesting from the geophysical viewpoint, but also encouraging from the engineering viewpoint.

The spin and the precession axes of the Earth have 23.5 degrees, but here we restrict ourselves to the case that they are at right angles for simplicity. On the other hand, although the main target in geophysics is the case of a large

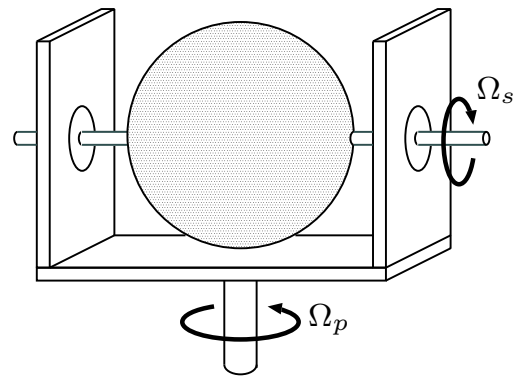


Figure 1: Schematic picture of a biaxially rotating sphere. The horizontal rotation axis is called the spin axis, whereas the vertical axis is called the precession axis because the sphere is precessing; i.e. the spin axis rotates around the precession axis. We deal with only the case that the two axes are at right angles.

Reynolds number (see (4) below for the definition) of $O(10^9)$ and a weak precession rate (see (5) below) of $O(10^{-7})$, we investigate the cases of various combinations of the parameters which are available in the laboratory or the numerical experiments.

CONTROL PARAMETERS

The Navier-Stokes equation nondimensionalised (for the length-scales by the sphere radius a , and for the time-scales by Ω_s^{-1}) is written as

$$\frac{\partial}{\partial t} \mathbf{u} + \mathbf{u} \cdot \nabla \mathbf{u} = -\nabla p + \frac{\nu}{a^2 \Omega_s} \nabla^2 \mathbf{u} + 2 \frac{\Omega_p}{\Omega_s} \mathbf{u} \times \hat{\mathbf{e}}_p \quad (1)$$

in the non-inertial frame rotating at the constant angular velocity Ω_p around the vertical axis. Here, \mathbf{u} and p are respectively the dimensionless velocity and pressure (including the centrifugal potential), and $\hat{\mathbf{e}}_p$ denotes the unit vector in the direction of the precession axis. The boundary condition is expressed as

$$\mathbf{u} = \hat{\mathbf{e}}_s \times \mathbf{x} \quad (2)$$

on the internal wall of the sphere. In (2), $\hat{\mathbf{e}}_s$ is the unit vector in the direction of the spin axis. Equations (1) and (2) together with the equation of continuity

$$\nabla \cdot \mathbf{u} = 0 \quad (3)$$

describe the motion of an incompressible viscous fluid in the precessing sphere. Therefore, only the two parameters, i.e. the Reynolds number

$$Re \equiv \frac{a^2 \Omega_s}{\nu}, \quad (4)$$

ν being the kinematic viscosity of fluid, and the ratio

$$\Gamma \equiv \frac{\Omega_p}{\Omega_s} \quad (5)$$

of two angular velocities characterise this system. Hereafter, we call Γ the precession rate (or the Poincaré number).

LABORATORY EXPERIMENT

Experimental Apparatus

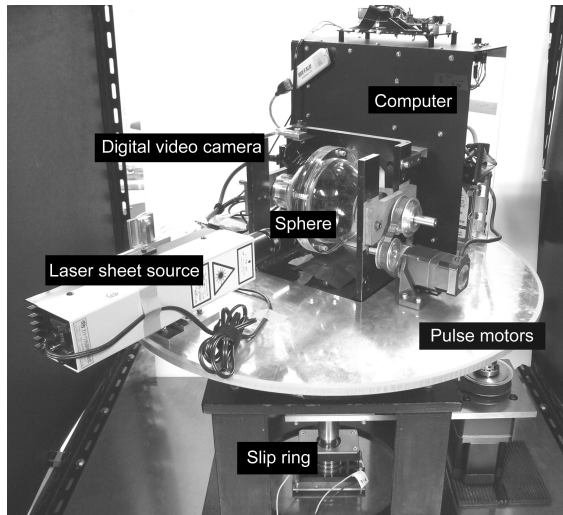


Figure 2: Experimental apparatus. A spinning acrylic sphere, a pulse motor, a laser light source, a small digital video camera and a computer for storing image data are fixed on the turntable. The turntable is rotated by another pulse motor fixed in the laboratory.

First, we experimentally investigate how the flow state inside the sphere changes depending on the two control parameters (Re, Γ). For this purpose, we have constructed (see Goto *et al.* 2007) an experimental apparatus shown in Fig. 2. The acrylic sphere of radius 50 mm is filled with degassed tap water, and the two rotations are driven by a couple of pulse motors, and therefore the control of the angular velocities is very precise. The angular velocities can be set in the range $\Omega_s/(2\pi) = 0.1 \sim 0.6$ Hz (which corresponds to the range $Re \approx 1500 \sim 9000$) and $\Omega_p/(2\pi) = 0.002 \sim 1.2$ Hz. Thanks to the precise control of the angular velocities, we have confirmed good flow reproducibility.

In our apparatus, a laser sheet source and a digital video camera are fixed on the turntable which rotates with the sphere around the precession axis. The video images are stored in a computer which are also set on the turntable. Electric power for the camera, the pulse motor and the computer is supplied through a slip ring. Thus, all the measurements described below are made in the precession frame

(i.e. the frame where (1) holds). The laser sheet is fixed perpendicular to the spin axis, and the perspective of the camera is approximately parallel to the spin axis. The centre of the sphere is not located on the light sheet, but about 17 mm behind the sheet. The digital camera records the motion of tracers (Kanomax ORGASOL; mean mass density and radius are 1.03 g/cm³ and 50 μ m, respectively.) in the thin (about 1 mm) laser sheet. We employ the particle image velocimetry (PIV) to measure the two-dimensional velocity field in the region of size 40 mm width by 24 mm height on the laser sheet. The measurements are carried out after more than $100T_s$, where $T_s = 2\pi/\Omega_s$ is the spin period, from the moment when Ω_s and/or Ω_p are changed impulsively.

Phase Diagram

It is observed in the visualisations shown in Fig. 3 that for a fixed $Re \approx 3500$, as Γ increases from 0, the flow changes as (i) the solid-body rotation around the spin axis (Fig. 3a), (ii) a steady swirling flow around an axis which is tilted around the precession axis (Fig. 3b), (iii) a periodic flow (Fig. 3c), (iv) turbulence (Fig. 3d) and (v) a steady swirling flow around the vertical axis (Fig. 3e). Here, recall that the centre of the sphere is not on the laser sheet but behind the sheet. Therefore, the tilt of the swirling flow is observed in Fig. 3(b) as the leftward shift of the circulation centre, and the circulation around the precession axis is observed in Fig. 3(d) as the rightward flow.

The transitions in the flow state observed in Fig. 3 are qualitatively understood as follows. First, it is analytically shown that the flow inside a sphere rotating at a constant angular velocity (that is, when either Ω_s or Ω_p vanishes) settles down to a solid-body rotation sooner or later. Second, when we add a weak precession (Fig. 3b), the solid-body rotation around the spin axis is weakly tilted by the Coriolis effect. The tilt angle is analytically derived by Busse (1968). This tilted swirling flow is accompanied with a boundary layer where the Coriolis force balances the viscous force. When the precession rate is strengthened, the balance might be unstable, and the flow becomes turbulent (Fig. 3d) through a periodic flow (Fig. 3c). If we further increases the angular velocity of the rotation around the precession axis, the flow relaminarises (Fig. 3d). For $\Gamma \gg 1$, it tends to make the solid-body rotation around the precession axis.

In order to unambiguously classify the flows inside the sphere into steady, periodic and turbulent, we estimate the two-time correlation function

$$C_i(\mathbf{x}, \tau) = \frac{\langle [u_i(\mathbf{x}, t) - \mu_i(\mathbf{x})][u_i(\mathbf{x}, t + \tau) - \mu_i(\mathbf{x})] \rangle}{\sigma_i^2(\mathbf{x})} \quad (6)$$

of a component u_i ($i = 1$ denotes the horizontal component, and $i = 2$ the vertical component) of the fluid velocity at the position \mathbf{x} measured by PIV. In (6), brackets $\langle \cdot \rangle$ denote the temporal average, and $\mu_i(\mathbf{x})$ and $\sigma_i(\mathbf{x})$ are respectively the mean and the standard deviation of $u_i(\mathbf{x}, t)$. The spatial (over the measurement plane) and ensemble averaged two-time correlation function \overline{C}_1 is plotted in Fig. 4 for three different precession rates Γ at a fixed Reynolds number $Re \approx 4700$. We can observe different behaviours of the correlation function depending on Γ . Here, we assume that the measured velocity is the superposition of the signal and noise which is statistically independent of the signal. Then,

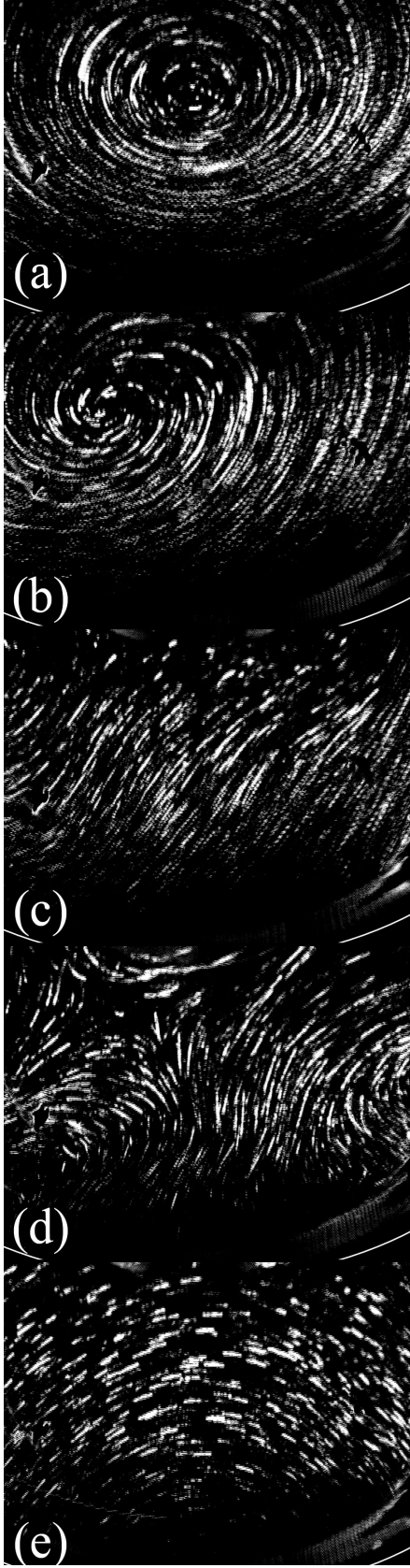


Figure 3: Flow visualisation in the precession frame. $Re \approx 3500$. (a) $\Gamma = 0$, rigid-body rotation. (b) 0.025, steady flow. (c) 0.05, periodic flow. (d) 0.2, turbulence. (e) 0.4, steady flow.

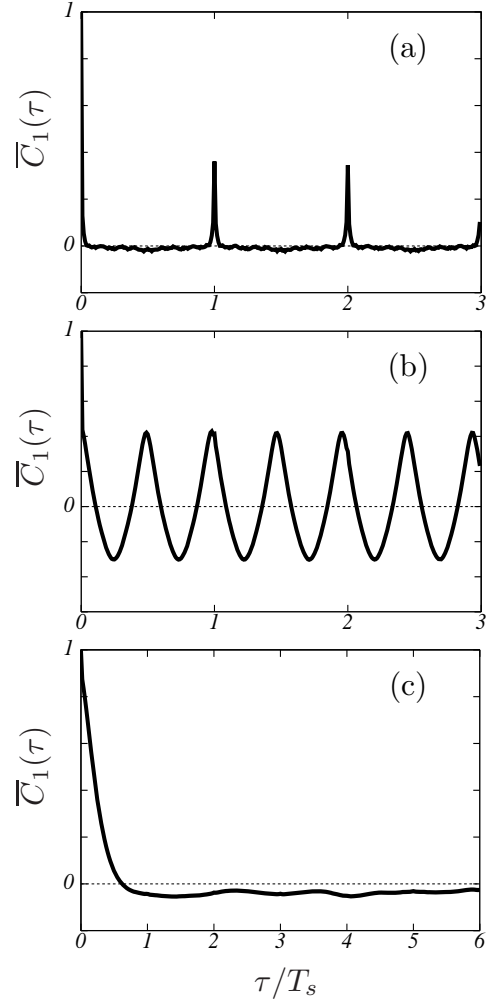


Figure 4: Two-time correlation function of the horizontal velocity component. Averaged value over the space and realisations is plotted. $Re \approx 4700$. (a) $\Gamma = 0$, (b) 0.04, and (c) 0.1.

the estimated correlation function is expressed as

$$C_i(\tau) = \frac{\tilde{\sigma}_i^2}{\tilde{\sigma}_i^2 + \sigma_i'^2} \tilde{C}_i(\tau) + \frac{\sigma_i'^2}{\tilde{\sigma}_i^2 + \sigma_i'^2} C_i'(\tau), \quad (7)$$

where \tilde{C}_i (or C_i') and $\tilde{\sigma}_i$ (or σ_i') are the two-time correlation function and standard deviation of signal (or noise), respectively. Therefore, from the correlation function observed in Fig. 4(a), we may conclude that the flow is steady because observed correlation function is only C_1' (note that $\tilde{\sigma}_1 = 0$ in the steady case). The correlation function of the noise has peaks at nT_s ($n = 0, 1, 2, \dots$). This correlation is due to the fact that since the sphericity of the cavity is not exact, the refraction of the laser sheet and the perspective of the camera changes periodically with the period T_s of the spin. Next, from Fig. 4(b), the flow is classified as periodic, because the observed correlation function is the superposition of the periodic function and the correlation of the noise which is observed in (a). Finally, the correlation function observed in Fig. 4(c) is obviously different from those in (a) and (b). Therefore, the flow is neither steady nor periodic. Here, such an aperiodic flow is classified as turbulence.

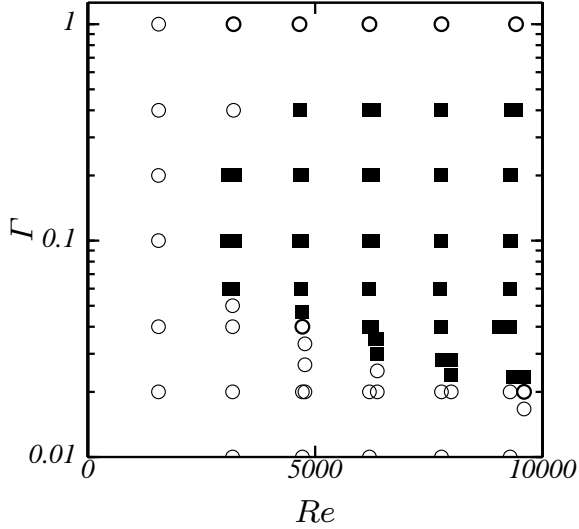


Figure 5: Phase diagram. Parameter sets to sustain turbulence are indicated by ■. Open circles denote the parameters for steady or periodic flows.

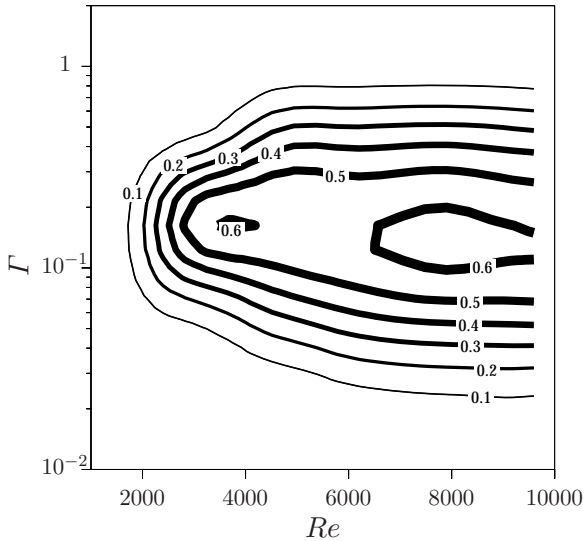


Figure 6: Spatial and ensemble averaged degree of turbulence.

Based on the above criterion, we have classified the flow sustained in the sphere for various combinations of Re and Γ . The result is shown in Fig. 5. It is worth emphasizing that turbulence is generated and sustained in the range that $O(0.1) \lesssim \Gamma \lesssim O(1)$ for $Re \gtrsim 3000$, and that if the Reynolds number is sufficiently large, turbulence is realised in the sphere with very small Γ . This is in contrast to the fact that turbulence is never generated by a steady rotation around a single axis.

Degree of Turbulence

In the preceding subsection, it has been shown that turbulence can be easily sustained in the sphere. Through the

extensive parameter survey, we have realised that the degree of the sustained turbulence drastically changes depending on the control parameters. In order to demonstrate this character of the system quantitatively, we estimate the degree of turbulence at position \mathbf{x} by

$$I(\mathbf{x}) = \sqrt{\langle |\mathbf{u}(\mathbf{x}, t) - \langle \mathbf{u}(\mathbf{x}) \rangle|^2 \rangle} / \sqrt{\langle |\mathbf{u}(\mathbf{x})|^2 \rangle} \quad (8)$$

for each parameter set for which turbulence is sustained (the parameters plotted by black squares in Fig. 5). Then, the contours of their spatial and ensemble averaged values \bar{I} are plotted in Fig. 6. It is observed that the degree of turbulence for a fixed Reynolds number is maximised when the precession rate Γ is around 0.1. This is because when Γ is much larger (or smaller) than this value, the turbulent flow is accompanied with the mean flow around the precession (or spin) axis. When $\Gamma \approx 0.1$, on the contrary, the sustained turbulence looks statistically homogeneous and isotropic without mean flow in the frame of reference (the precession frame).

Since the tune of the control parameters of the present system is precise, the above result that the degree I of sustained turbulence drastically depends on the parameters implies the possibility of the precise control of I . This feature of the present system might well be an advantage when applying it to a mixer, for example.

DIRECT NUMERICAL SIMULATION

Numerical Scheme

Since it is difficult to experimentally investigate the detailed three-dimensional flow structure inside a sphere, we conduct a highly precise DNS employing a spectral method. Here, we adopt spherical harmonic functions in the direction of (θ, ϕ) in the spherical coordinate (r, θ, ϕ) and a kind of Jacobi polynomials (Matsushima and Marcus 1995) in the r direction. As emphasised above, since there are only two control parameters Re and Γ in this system, and since the boundary condition is extremely simple, we can carry out the DNS which precisely corresponds to the laboratory experiment for the same set of parameters (Re, Γ) .

In the DNS, the velocity field \mathbf{u} is expressed in terms of two scalar functions Ψ and Φ as

$$\mathbf{u} = \nabla \times (\Psi \mathbf{x}) + \nabla \times \nabla \times (\Phi \mathbf{x}), \quad (9)$$

which ensures the incompressibility (3) of the fluid. Then, the governing equations for these scalar functions are numerically integrated by the combination of the second-order Adams-Bashforth and the Crank-Nicolson schemes. The numbers of the collocation points in the spectral method are set as 64, 128 and 256 in the r , θ and ϕ directions, respectively. The details of the numerical scheme are given in Kida and Nakayama (2007).

Comparison with Experiment

In order to verify that the present DNS reproduces flows consistent with the laboratory experiment, we show here a result of the DNS for the same parameter set as shown in Fig. 4(b), i.e. $Re = 4720$ and $\Gamma = 0.04$. The temporal evolution of a velocity component at a position is shown in Fig. 7 for the duration $0 \leq t \leq 130T_s$. After a long transient period of $O(100T_s)$, the system finally approaches a periodic flow with a period $0.49T_s$. This coincides with the period observed in the experiment (Fig. 4b). The period estimated

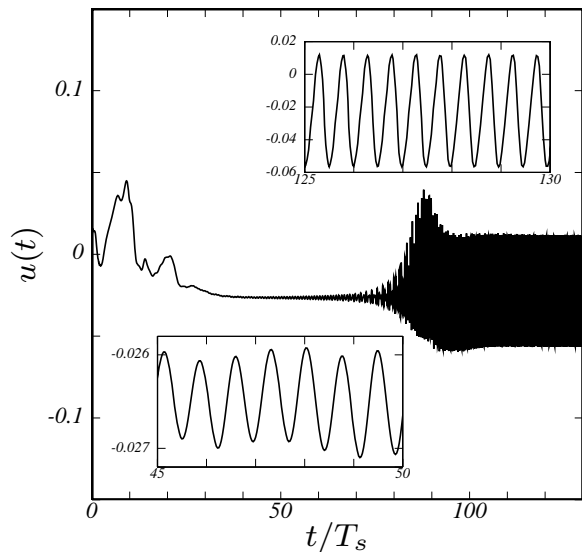


Figure 7: Temporal evolution of a velocity component at a position. $Re = 4720$, $\Gamma = 0.04$. DNS result.

by the Fourier transform of the correlation function shown in Fig. 4(b) is about $0.48T_s$. It is further interesting to observe that the system experiences a transient plateau ($30T_s \lesssim t \lesssim 70T_s$) before reaching the final periodic state. In this plateau, the flow is also periodic but the period is about $0.72T_s$ (about 1.5 times longer than the final period). This behaviour is not unique for this parameter, but observed also for other parameters. We suppose that the secondary flow developing for $t \lesssim 40T_s$ modifies the primary flow, and then the modified primary flow triggers another instability which leads to the final state.

We have also estimated numerically the critical Reynolds numbers Re_c , at which the steady flow becomes unstable and a periodic flow appears (the present laboratory experiments show that the laminar-turbulent transition in the low Γ range always experiences a Hopf bifurcation), for each value of Γ in the range $0.04 \leq \Gamma \leq 1.6$. The result is consistent with the phase diagram (Fig. 5) obtained by the laboratory experiment. However, it is revealed by the DNS that $Re_c(\Gamma)$ is not a monotonic function of Γ , but complicated. This may imply that the most unstable mode changes as a non-trivial function of Γ .

Three-dimensional Flow Structure

An advantage of DNS is that we can capture easily details of flow structure. We visualise in Fig. 8 the velocity field of the flow for the parameter sets ($Re = 4720$, $\Gamma = 0.04$) shown in the preceding subsection. Figure 8(a) shows the velocity field on the $Z = 0$ plane, where Z is in the direction of the precession axis and the origin is at the centre of the sphere, at a time ($t = 40T_s$) during the plateau shown in Fig. 7, whereas (b) shows the velocity field on the same plane at a time ($t = 136$) in the final periodic state. It is seen that the overall flow structure is almost the same at these two times; that is, we can observe a clockwise swirl at the centre of the sphere, and four pairs of peripheral eddies. The positions of these eddies are almost stationary in both cases, but the shape periodically changes for $t \gtrsim 100T_s$. Therefore, the observed oscillation for $t \gtrsim 100T_s$ may be understood in

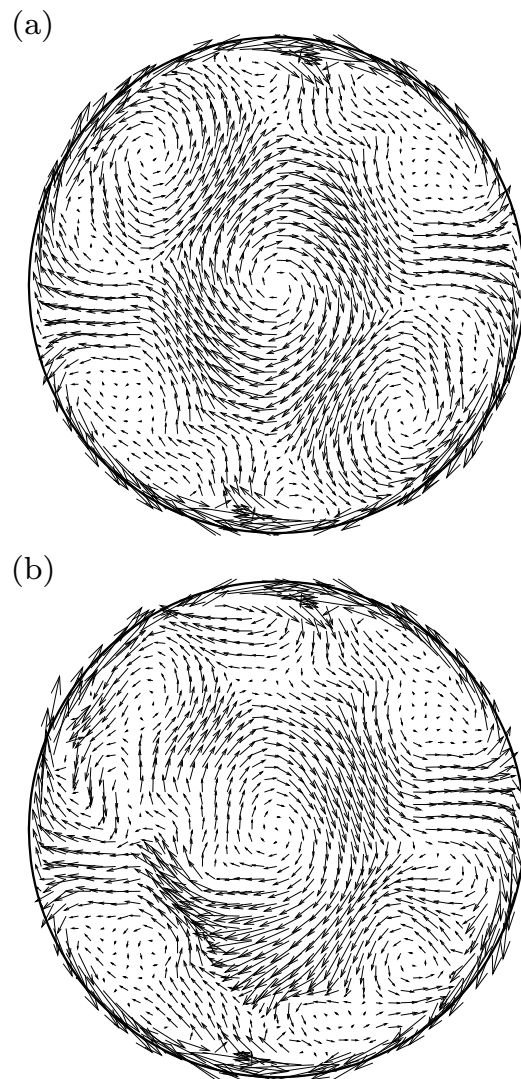


Figure 8: Velocity field on the $Z = 0$ plane. Z is in the direction of the precession axis. The horizontal direction is parallel to the spin axis. $Re = 4720$, $\Gamma = 0.04$. DNS result. (a) $t = 40T_s$. (b) $t = 136T_s$.

terms of the secondary instability of the mean flow, which is created by the nonlinear saturation of the initial instability for the duration $t \lesssim 40T_s$.

It is an important near-future problem to investigate numerically the details of statistics and three-dimensional structures of developed turbulence sustained inside the sphere when $Re \gtrsim 3000$ and $\Gamma = O(0.1)$. However, we have found that even in small Reynolds numbers the steady flows inside the sphere have non-trivial flow structures. Two streamlines in the steady flow at $Re = 10$ and $\Gamma = 0.1$ are shown in Fig. 9. Each of these streamlines is very dense in the space and constitutes a torus. By a detailed Poincaré-section analysis of streamlines, it is seen that this steady flow consists of four separate regions, and that the streamline topology is sensitive to Re and Γ . These flow structures at low Reynolds numbers may be important when applying this flow system to a kind of gentle mixer relying on the Lagrangian chaos.

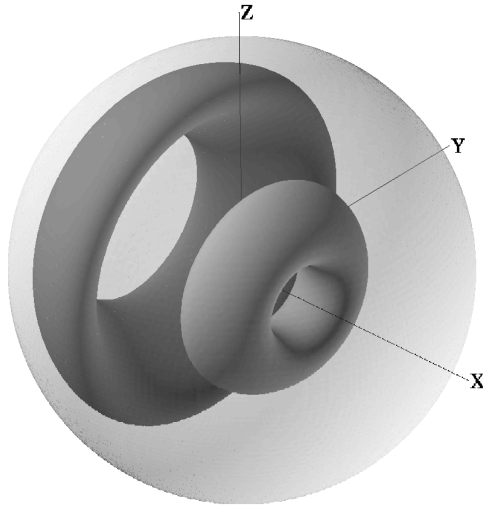


Figure 9: Two streamlines of a steady flow ($Re = 10$, $\Gamma = 0.1$). Each of streamlines constitutes a torus. X and Z denote the directions of the spin and the precession axes, respectively.

CONCLUSION

Using a biaxially rotating sphere, we have proposed a turbulence generator. This generator may possess some desirable features. First, in contrast to experiments in a wind tunnel, the system is closed and without free boundary affecting the flow. Secondly, in contrast to turbulence experiments using stirrers, the boundary condition is extremely simple. Not only flow state (steady, periodic or turbulent) but also the degree of turbulence inside the sphere are perfectly controlled only by the two parameters Re and Γ . The simpleness of the boundary conditions also permits us to conduct the DNS under the precisely same condition as the laboratory experiment. Furthermore, since large-scale eddies induced by the spin easily break up to smaller eddies by the relatively weak action of the precession, we can sustain fully developed turbulence inside the sphere easily. These facts (the smallness of the number of control parameters and the easiness in sustaining turbulence) imply the possibility that this system serves as a *standard tabletop turbulence generator* which may be useful for discussions (on the validity of turbulence models, e.g.) among researchers in different laboratories.

This study is supported by the 21st Century COE Program on Complex Functional Mechanical Systems, and Grants-in-Aid from the Ministry of Education, Culture, Sports, Science and Technology. The DNS was carried out on NEC SX-8 at YITP in Kyoto University and on NEC SX-8/32M4 at National Institute for Fusion Science by the support of the collaborative program.

REFERENCES

- Busse, F. H. 1968, "Steady fluid flow in a precessing spheroidal shell," *J. Fluid Mech.*, Vol. 33, pp. 739–751.
- Goto, S., Ishii, N., Kida, S. and Nishioka, M. 2007, "Turbulence Generator Using a Precessing Sphere," *Phys. Fluids*, in press.
- Hollerbach, R. and Kerswell, R. R. 1995, "Oscillatory internal shear layers in rotating and precessing flows," *J. Fluid*

Mech., Vol. 298, pp. 327–339.

Kerswell, R. R. 1995, "On the internal shear layers spawned by the critical regions in oscillatory Ekman boundary layers," *J. Fluid Mech.*, Vol. 298, pp. 311–325.

Kida, S. and Nakayama, K. 2007, "Helical flow structure in a precessing sphere," in preparation.

Kobine, J. J. 1995, "Inertial wave dynamics in a rotating and precessing cylinder," *J. Fluid Mech.*, Vol. 303, pp. 233–252.

Kobine, J. J. 1996 "Azimuthal flow associated with inertial wave resonance in a precessing cylinder," *J. Fluid Mech.*, Vol. 319, pp. 387–406.

Lorenzani, S. and Tilgner, A. 2001, "Fluid instabilities in precessing spheroidal cavities," *J. Fluid Mech.*, Vol. 447, pp. 111–128.

Malkus, W. V. R. 1968, "Precession of the earth as the cause of geomagnetism," *Science*, Vol. 160, pp. 259–264.

Manasseh, R. 1992, "Breakdown regimes of inertia waves in a precessing cylinder," *J. Fluid Mech.*, Vol. 243, pp. 261–296.

Matsushima, T., and Marcus, P. S. 1995, "A spectral method for polar coordinates," *J. Comp. Phys.*, Vol. 120, pp. 365–374.

Noir, J., Cardin, P., Jault, D. and Masson, J.-P. 2003, "Experimental evidence of nonlinear resonance effects between retrograde precession and the tilt-over mode within a spheroid," *Geophys. J. Int.*, Vol. 154, pp. 407–416.

Noir, J., Jault, D. and Cardin, P. 2001, "Numerical study of the motions within a slowly precessing sphere at low Ekman number," *J. Fluid Mech.*, Vol. 437, pp. 283–299.

Tilgner, A. and Busse, F. H. 2001, "Fluid flows in precessing spherical shells," *J. Fluid Mech.*, Vol. 426, pp. 387–396.

Vanyo, J. P. and Dunn, J. R. 2000, "Core precession: flow structures and energy," *Geophys. J. Int.*, Vol. 142, pp. 409–425.

Vanyo, J., Wilde, P., Cardin, P., and Olson, P. 1995, "Experiments on precessing flows in the Earth's liquid core," *Geophys. J. Int.*, Vol. 121, pp.136–142.